A major purpose of the Technical Information Center is to provide the broadest dissemination possible of information contained in DOE's Research and Development Reports to business, industry, the academic community, and federal, state and local governments.

Although a small portion of this report is not reproducible, it is being made available to expedite the availability of information on the research discussed herein.

LA-UR -87-56

LA-UR--87-56

DE87 005117

Los Alamos National Laboratory is operated by the University of California for the United States Department of Energy under contract W-7405-ENG-36

TITLE: ISOVECTOR RESONANCES IN PION SINGLE-CHARGE-EXCHANGE REACTIONS

AUTHOR(S): J. David Bowman, MP-4, Los Alamos National Laboratory

SUBMITTED TO: Proceedings of Workshop on Isospin Excitations in Nuclei
TRIUMF, Vancouver, B. C. Canada, October 7-8, 1986

DISCLAIMER

Los Alamos National Laboratory
Los Alamos, New Mexico 87545

FORM NO 836 R4
ST NO 2629 5/81

Isovector Resonances in Pion Single-Charge-Exchange Reactions

J. David Bowman

Los Alamos National Laboratory

Abstract

I report on the experimental study of $L = 0$, 1, and 2 isovector resonances in pion charge-exchange reactions.

I will discuss the results of a series of experiments carried out by a collaboration of Tel-Aviv University and Los Alamos National Laboratory, which studied the excitation of $L = 0$, 1, and 2 isovector giant resonances in pion charge-exchange reactions $(\pi^{\pm}, \pi^0)$. A complete account of this work has been given elsewhere (1)(2), and so I will not discuss experimental details, or complete describe the analysis procedure.

Giant resonances are excitations of the nucleus in which large numbers of nucleons move collectively. They are simple modes of nuclear excitation that can be interpreted microscopically or macroscopically. Their experimental observation and study as well as their theoretical interpretation are important for models of nuclear excitation and the knowledge of the nucleon-nucleon interaction in the nuclear environment. The experimental properties that characterize a giant resonance are the concentration of a large fraction of the total available transition strength with specific quantum numbers in a narrow region of excitation energy, the occurrence of resonances in a wide range of nuclei, and the smooth variation of excitation energy and width of the resonance with nuclear mass A. In contrast to the isoscalar electric modes, which have been extensively studied in the scattering of hadronic probes, the $L = 1$, $T = 1$ or giant dipole resonance (GDR), which has been studied with electromagnetic probes, and the $L = 0$, $T = 1$, $S = 1$ Gamow-Teller resonance, which has been studied in the (p, n) reaction, the $L = 0$ $T = 1$ isovector monopole resonance (IVM) and $L = 2$, $T = 1$ isovector quadrupole resonance (IVQ) were poorly characterized before pion charge-exchange studies. The study of

the IVM was of particular importance. Its existence had been predicted by both macroscopic (3) and microscopic (4) theories, but it had not been observed. The IVM plays a central role in Coulomb effects such as isospin mixing in nuclear ground states, Coulomb displacement energies and widths of analog states.

The quantum numbers and dynamical properties of resonance-energy pions make the pion charge-exchange reactions ($\pi^{\pm}, \pi^0$) ideal for the study of electric isovector resonance, especially the IVM. First, the use of a charge-exchange reaction that excites only isovector states eliminates the excitation of isoscalar states that dominate the excitation spectra of inelastic scattering processes. Second, at forward angles, where the angular distribution of the IVM peaks, pion charge exchange excites primarily electric, or non-spin-flip transitions (in contrast to the (p,n) reaction), reducing spin-flip backgrounds. Third, the strong absorption of the pion is essential for the excitation of a monopole state for which the volume integral of the transition density is zero. The angular distributions produced by the surface-related diffractive pion scattering process [similar to $((\alpha,\alpha')$] oscillate sharply and characteristically with angle (5).

$$\frac{d\sigma}{d\Omega} \sim J_0^2(kR\theta) \quad \text{for} \quad L=0$$
$$\frac{d\sigma}{d\Omega} \sim J_1^2(kR\theta) \quad \text{for} \quad L=1$$
$$\frac{d\sigma}{d\Omega} \sim J_0^2(kR\theta) + 3J_2^2(kR\theta) \quad \text{for} \quad L=2 \quad ,$$

where k is the π momentum, θ is the scattering angle and R is the strong absorption radius. This rapidly oscillating behavior serves to identify the

multipolarity of the transition and to distinguish the giant resonance signals from the nonresonant background. In Figure 1 representative angular distributions for the ^{60}Ni (π^-, π^0) reaction at 230 MeV are shown. The qualitative patterns of the angular distributions do not depend on the details of the reaction model used so long as the pion waves are strongly absorbed.

Fourth, the Coulomb energy shift for states populated by the (π^-, π^0) reaction is advantageous. This point is illustrated in Figure 2 where the analog state relations are shown for an isovector resonance built on a target ground state of isospin T. For nuclei with $T \gg 1$, transitions to the state of lowest total isospin are strongly favored by isospin coupling coefficients. The state of total isospin $T + 1$ in the (π^-, π^0) daughter is shifted down by the Coulomb displacement energy relative to its analog in the parent nucleus. Thus the $T + 1$ state has a relatively low excitation energy in the (π^-, π^0) daughter and occurs at an excitation energy where the density of states of the same isospin is small. The opposite situation pertains for the (π^+, π^0) reaction. The $T + 1$ component populated in the (π^-, π^0) reaction is expected to be narrow and to occur at a low excitation energy while the $T - 1$ component populated in the (π^+, π^0) reaction is expected to be wide and to occur at a high excitation energy.

In the experiments well-understood, spherical, even-even nuclei were studied in the $(\pi^\pm, \pi^0)$ reactions at 120, 165, and 230 MeV. The emphasis of the 165 MeV study, which was done first, was on $L = 0$, 1, and 2 isovector resonances as function of the atomic mass of the target. The

targets were ^{40}Ca, ^{60}Ni, ^{90}Zr, ^{120}Sn, ^{140}Ce, and ^{208}Pb. The 120- and 230-MeV studies were aimed at measuring the properties of the isovector resonances as functions of bombarding energy for a few targets, ^{40}Ca, ^{60}Ni, and ^{120}Sn. Double differential cross sections up to excitation energies of 60 MeV were measured out to angles extending well past the second maximum of the IVQ angular distribution. Data for the ^{120}Sn target with a 165 MeV π^- beam are shown in Figures 3a and 3b. At the most forward angle, 4.5°, the IVM cross section is expected to be the largest. The second angle, 11°, is chosen to be near the first minimum of the monopole angular distribution. The GDR cross section is small at the forward angle and has a maximum near 11°. Figure 3c shows the results of subtracting the 11° spectrum from the 4.5° spectrum. This subtraction suppresses the approximately isotropic non-resonant background. The IVM signal is the positive-going hump and the small GDR signal is the negative-going hump.

The above analysis shows the existence of peaks above an approximately isotropic background in the $d^2\sigma/d\Omega dE$ versus pion kinetic energy spectra. The IVM peak is visible in a comparison of the 4.5° and 11° spectra but the GDR peak is not. The subtraction procedure makes the weak GDR peak visible. To investigate the degree of isotropy of the non-resonant background it is necessary to look at the dependence of different regions of excitation energy on scattering angle or momentum transfer q. Figure 4 shows the forward-angle data for ^{60}Ni (π^-, π^0) taken at 230 MeV. As before, the IVM is large in the most forward angle where the GDR is

small. The IVM is small at the second angle where the GDR is large and both are small at the largest angle. In general cross sections depend on energy loss ν and momentum transfer q^2. Figure 5 shows $d\sigma/d\Omega$ obtained by integrating over the three regions indicated in Figure 4. Region one emphasizes the IVM, region two emphasizes the GDR and region three contains mostly nonresonant background. Each plot can be represented as a superposition of a background linear in q^2 and a component having the q^2 dependence expected for $d\sigma/d\Omega$ for a $L = 0$ or 1 resonance. Although the background is not strictly isotropic its dependence on q^2 is much less rapid than that of the giant resonances.

In order to extract quantitatively excitation energies, widths, and maximum cross section, a least-squares fitting procedure was followed. The double differential cross section as a function of q^2 and ν was written as a sum of two Gaussian peaks at an angle-independent excitation energy. The q^2 variation of the peaks was taken to be that of distorted wave impulse approximation calculations using random-phase-approximation (RPA) (6) transition densities. The sizes of the maximum cross sections were varied. The background was written as a function having a smooth ν-dependence and a quadratic q^2-dependence. Resonance and background parameters were varied to fit the data for each target. The background function and the resonance components shown in Figure 4 were obtained in this way.

Figure 6 shows the extracted maximum cross sections, excitation energies, and widths for the IVM and GDR resonances extracted from the

165-MeV data. Results of random-phase-approximation distorted-wave-impulse-approximation (RPA-DWIA) calculations (6) are also shown.

The A-dependence of the 1 $\hbar\omega$ GDR cross sections can be understood as follows. In the (π^-, π^0) reaction a proton is turned into a neutron and is promoted by one major shell. For the $T = 0$ nucleus, ^{40}Ca, there is no blocking and the π^+ and π^- cross sections are comparable. For ^{208}Pb the neutron shell is fully occupied and the (π^-, π^0) cross section for the GDR is zero. The same effect is seen to a lesser extent for the A-dependence of the 2 $\hbar\omega$ IVM maximum cross sections. Here the (π^-, π^0) IVM cross sections decrease by about a factor of two from ^{40}Ca to ^{208}Pb while the (π^+, π^0) IVM cross sections are approximately constant. As expected, the widths and excitation energies of $T + 1$ states are larger than those of the corresponding $T - 1$ states. Where data are available from other reactions, they are also shown. The solid curves give the theoretical results for multipole strength weighting and the dashed curves give the results for cross section weighting. The cross-section-weighted RPA theory using the Skyrme III residual interaction (6) gives a reasonable description of the data.

Remarkably, no IVQ peak was necessary to fit the experimental double differential cross section data. In order to quantify the amount of IVQ cross section present in the data, a third Gaussian peak was added to the fitting function. The excitation energy, width, and q^2-dependence of the peak were taken from RPA-DWIA calculations. The data were refitted and 90% confidence level upper limits were deduced for the presence of

an IVQ component. These upper limits were 0.18, 0.30, and 0.15 of the RPA-DWIA estimate of the peak IVQ cross section for ^{40}Ca, ^{60}Ni, ^{90}Zr (π^-, π^0) respectively. For the IVM and GDR the observed cross sections were typically 0.7 of the RPA-DWIA calculations. If a much larger width was assumed the upper limit for the IVQ cross section was increased and became consistent with the RPA-DWIA estimate.

An interesting explanation of the absence of isovector quadrupole strength in the pion charge-exchange reaction has been proposed by Leonardi *et al.* (7). They argue in a sum-rule framework that the inclusion of non-local terms in the residual interaction would have little effect on the properties of $L = 0$, 1, and 2 isovector giant resonances in $\Delta T_z = 0$ channels, and on the properties of the $L = 0$ and $L = 1$ isovector resonances in charge-exchange channels. Thus RPA calculations with local interaction could correctly describe these properties of these isovector giant resonances even if the true residual interaction were non-local. However, Leonardi *et al.* argue that the inclusion of non-local residual interaction could radically broaden and weaken the isovector quadrupole resonance in the charge-exchange channels. The absence of isovector quadrupole strength in the pion charge-exchange reactions has been a problem and Leonardi's explanation is intriguing.

As noted above, experiments were carried out for 120-MeV and 230-MeV pion energies as well as at 165 MeV. A test of the hypothesis that the bumps in the cross section data that have been identified as giant resonances are indeed giant resonances is provided by the lack of dependence

on bombarding energy of extracted excitation energies and widths. Figure 7 shows the extracted excitation energies and widths for ^{40}Ca, ^{60}Ni, and ^{120}Sn as functions of bombarding energy for π^+ and π^- projectiles. These quantities are indeed independent of projectile energy. Other tests of the giant resonance interpretation of the data are provided by the angular distributions of the bumps.

The forms $J_0^2(qR)$ and $J_1^2(qR)$ with $R = 1.37\,A^{1/3}$ fm are good approximations to the DWIA calculations for monopole and dipole states, respectively. Experimental data[8] for $\pi^\pm$ elastic-scattering angular distributions at 180 MeV from a wide range of nuclei can be described by the form $d\sigma/d\Omega \simeq J_1^2(qR)/(qR)^2$, where the strong-absorption radius is given by $R = 1.37\,A^{1/3}$. To test the suitability of the angular distributions for the giant resonances that we assumed in the extraction of the resonance parameter, we performed fits using the following forms for the angular distribution of the monopole and dipole states,

$$J_0^2[2kR\sin(\theta/2)] \quad \text{for monopole,}$$

and

$$J_1^2[2kR\sin(\theta/2)] \quad \text{for dipole,}$$

with R as a free parameter. The fitted values of R agreed with $R = 1.37\,A^{1/3}$ within the 10% errors to which they were determined. The mass dependence of the extracted interaction radii is given in Figure 8.

The angular distribution for the monopole and dipole are expected to shift forward as the momentum of the projectile is increased. The

position of the first minimum in the angular distribution of the monopole and dipole can be obtained from the fitted value of R from the relations

$$X_0^0 = 2kR\sin(\theta_{\min}/2) \quad \text{for the monopole}$$

and

$$X_0^1 = 2kR\sin(\theta_{\min}/2) \quad \text{for the dipole,}$$

where $X_0^0 = 2.40$ is the first zero of $J_0(X)$ and $X_0^1 = 3.83$ is the second zero of $J_1(X)$. In Figure 7 we plot values for $\theta_{\min}$ for the monopole and dipole resonances excited in the (π^-, π^0) reaction for ^{60}Ni as functions of the inverse of the momentum of the incident pion. The monopole and dipole angular distributions do indeed shift to more forward angles as the incident pion momentum increases. The solid lines shown in Figure 9 represent the prediction of the above relations for $\theta_{\min}$ with $R = 1.37\,A^{1/3}$. The angular distributions for the monopole and dipole shift forward in the way expected from surface-related diffractive scattering with a constant interaction radius.

For a strongly absorbed probe, such as the pion in the (3,3) resonance region, one expects surface-related diffractive scattering. Following the ideas developed in Ref. 9 it is possible to show that the energy dependences of the 0° cross section for the isobaric-analog state, the monopole resonance, and the maximum cross section for the dipole resonance should all be approximately the same and should be proportional to

$$d\sigma/d\Omega_{\max} \sim \frac{d\sigma/d\Omega(\pi^- p \to \pi^0 n)}{d\sigma/d\Omega(\pi^- p \to \pi^- p) + d\sigma/d\Omega(\pi^+ p \to \pi^+ p)} k^2 \quad .$$

This formula shows that the size of the cross section is determined by the competition between the pion-nucleon charge-exchange cross section, the numerator, and the isospin averaged pion-nucleon total cross section, the denominator. In the neighborhood of the (3,3) resonance the ratio of these cross sections is constant, so the maximum cross sections to the isobaric-analog state and the resonances are all predicted to increase as k^2.

The most complete experimental data for the 0° cross section of the isobaric-analog state in this mass and energy range are for ^{120}Sn and ^{60}Ni. These data are shown in Figure 10. We also show the prediction of the fits to the systematic behavior of the isobaric-analog state using the formula given in Sennhauser *et al.*[10] For ^{40}Ca we show the prediction from systematics for ^{42}Ca for which an isobaric-analog state exists. The maximum differential cross sections for the monopole and dipole states as functions of bombarding energy are shown in Figure 10. The monopole and dipole maximum cross sections increase as the energy increases. The increase is similar from nucleus to nucleus for the two incident pion charges and for the monopole and dipole resonances. From 120 to 165 MeV the maximum cross section of the isobaric-analog state increases in the same way that the maximum cross sections for the monopole and dipole resonances increase. From 165 MeV to 230 MeV the increase of the isobaric-analog-state maximum cross sections is less than those for the monopole and dipole resonances. The energy dependence of the resonance cross sections is close to expectation based on the distorted-wave Born approximation.

The energy dependence of the isobaric-analog-state cross section is different than these expectations. This fact suggests that there is some aspect of the calculation of isobaric-analog state cross sections which has been overlooked. Differences between the energy dependences of analog and nonanalog transitions have been observed in pion double-charge exchange.[11] An explanation in terms of two interfering amplitudes has been proposed.[12]

I have described a series of experiments which observed and studied the properties of the isospin components of the giant dipole and isovector monopole resonances in pion charge-exchange reactions. The isovector dipole and isovector monopole energies, widths, and cross sections were found to be in agreement with the predictions of RPA-DWIA calculations. The strong-interaction radii for the monopole and dipole states extracted in a Bessel-function analysis agree with those found in elastic pion scattering. The angular distribution for the monopole and dipole states shifts forward in angle as the momentum of the incident pion is increased, as expected for surface-related diffractive scattering with constant strong interaction radius. The variations of excitation energy, width, and maximum cross section with atomic mass at fixed pion energy was determined. The excitation energy, width, and maximum cross section were found to be independent of bombarding energy for a few targets, providing a test of the analysis procedure. The excitation energy and width of the states have a smooth dependence on the mass of the target and are in agreement with RPA calculations. The cross sections of the states exhaust approximately 0.7 of the RPA-DWIA calculations. The maximum

cross section for the monopole peak changes with energy in the same way as the maximum cross section for the dipole peak changes and in the way expected for surface-related diffractive scattering of resonance-energy pions. Much less isovector quadrupole strength than expected from RPA-DWIA calculations and much less strength than displayed in observations of the isovector monopole and dipole resonance were found. The energy dependence of the maximum cross sections for the dipole and monopole resonances were found to increase as k^2 as the bombarding energy was increased. The isobaric-analog-state cross sections increased slower than k^2 between 165 and 230 MeV, indicating some problem in the distorted-wave Born approximation treatment of the reaction mechanism or in the structure of the isobaric-analog state.

References

1. A. Erell *et al.*, Phys. Rev. **C34**, 1822 (1986).
2. F. Irom *et al.*, Phys. Rev. **C34**, 2231 (1986).
3. A. Bohr and B. R. Mottelson, Nuclear Structure (Benjamin, New York, 1975).
4. G. F. Bertsch and S. F. Tsai, Phys. Rev. **C18**, 125 (1975); K. F. Liu and G. E. Brown, Nucl. Phys. **A265**, 385 (1976); N. Auerbach, Nucl. Phys. **A182**, 247 (1972).
5. J. D. Bowman *et al.*, Phys. Rev. Lett. **46**, 1614 (1981); A. Gal, Phys. Rev. **C25**, 2680 (1982).

6. N. Auerbach and A. Klein, Phys. Rev. **C28**, 2075 (1983); N. Auerbach and A. Klein, Nucl. Phys. **A395**, 77 (1983); A. Klein, Ph.D. Thesis, Tel-Aviv University, 1984.
7. Leonardi *et al.*, preprint (submitted to Phys. Rev. Lett.).
8. R. Corfu *et al.*, in *Meson-Nuclear Physics—1979 (Houston)*, proceedings of the 2nd International Topical Conference on Meson-Nuclear Physics, AIP Conf. Proc. No. 54, edited by E. V. Hungerford III (AIP, New York, 1979); R. A. Eisenstein, *ibid.*
9. N. Auerbach, M. B. Johnson, A. Klein, and E. R. Siciliano, Phys. Rev. **C29**, 526 (1984).
10. U. Sennhauser *et al.*, Phys. Rev. Lett. **51**, 1324 (1983).
11. R. Gilman *et al.*, preprint (submitted to Phys. Rev. C) and references therein.
12. R. Gilman *et al.*, Nucl. Phys. **A432**, 610 (1985).

Figure Captions

Figure 1. Angular distribution for $L = 0$, 1, and 2 collective transitions for 230 MeV (π^-, π^0) reactions on ^{60}Ni.

Figure 2. Analog relationships for isovector resonances built on a $T \geq 1$ target nucleus.

Figure 3. Figures 3a and b show the double differential cross section as functions of T_{π^0} in the ^{120}Sn(π^-, π^0) reaction at a forward angle where the IVM cross section is large (a) and at a larger angle where the IVM cross section is small (b). Figure 7c shows the difference of the 4.5° and 11° spectra.

Figure 4. Double differential cross sections as functions of T_{π^0} for scattering angles of 4.5°, 15.0°, and 24.0° for the ^{60}Ni(π^-, π^0) reaction at 230 MeV.

Figure 5. Differential cross sections obtained by integrating over the T_{π^0} regions shown in Figure 4, as functions of momentum transfer squared. The solid lines are fits to a linear background added to a $L = 0$ or $L = 1$ angular distribution for the IVM and GDR respectively.

Figure 6. Extracted maximum cross sections, excitation energies, and widths for the GDR and IVM resonances The lines are the results of random phase approximation calculations done before the data were available.

Figure 7. Extracted excitation energies and widths for ^{40}Ca, ^{60}Ni, and ^{120}Sn $(\pi^{\pm}, \pi^0)$ reactions for the isovector monopole resonances (IVM) and giant dipole resonances (GDR) plotted versus the pion bombarding energy.

Figure 8. Pion interaction radii (R) extracted by fitting the angular distribution in the diffractive relations $J_l^2(qR)$. The straight lines connect the values extracted from π^+ and π^- elastic scattering at 180 MeV.

Figure 9. Location of the first minimum of the isovector monopole resonance and the second minimum of the isovector giant dipole resonances excited by the (π^-, π^0) reaction on ^{60}Ni versus the inverse of the momentum of the incident pions. The solid lines represent the prediction for the location of the minima for a constant interaction radius $R = 1.37\,A^{1/3}$ fm (see text).

Figure 10. Maximum cross sections for (π^+, π^0) and for (π^-, π^0) for the isovector monopole resonances, giant dipole resonances, and isobaric-analog states as a function of bombarding energy. For ^{60}Ni and ^{120}Sn experimental results of the 0° cross sections for the isobaric-analog state (IAS) from this work and Ref. 10 are plotted (closed circles points). Also shown are the expected values from systematics of the isobaric-analog state using the formula given in Ref. 10 (cross points). For

^{40}Ca there is no isobaric-analog state and the expected values from systematics of the isobaric-analog state for ^{42}Ca are plotted (cross points). Also shown are the energy dependence of the maximum cross sections for the monopole, dipole, and isobaric-analog state using the approximate expression discussed in the text (solid curve). The energy dependence for the monopole and dipole maximum cross sections are similar and they are the same as the energy dependence of the approximate expression (solid curve). The isobaric-analog-state maximum cross section increases less than the resonance cross sections from 165 to 230 MeV.

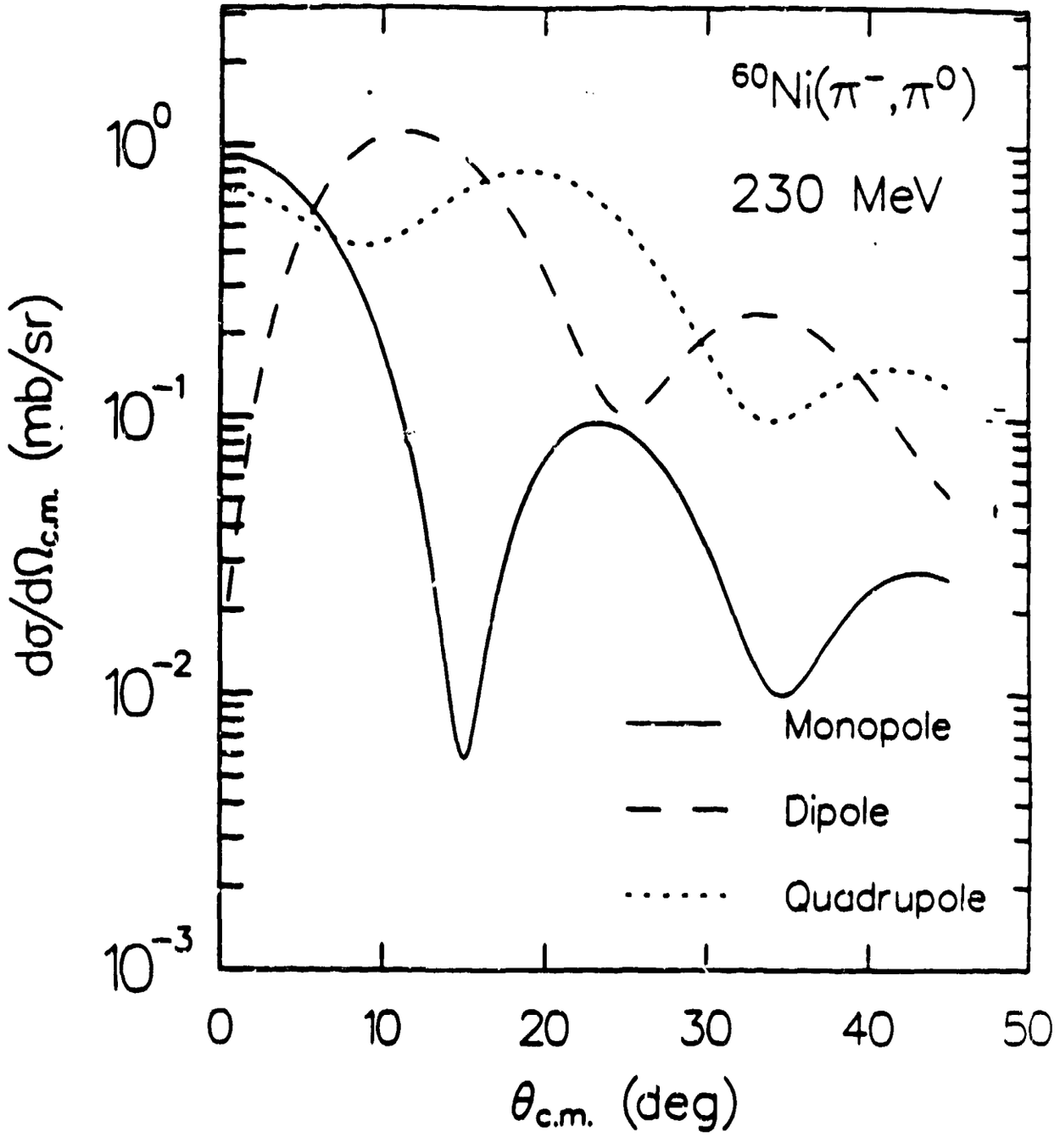
$^{60}Ni(\pi^-,\pi^0)$
230 MeV
Monopole
Dipole
Quadrupole
$d\sigma/d\Omega_{c.m.}$ (mb/sr)
10^0
10^{-1}
10^{-2}
10^{-3}
0
10
20
30
40
50
$\theta_{c.m.}$ (deg)

Fig 1

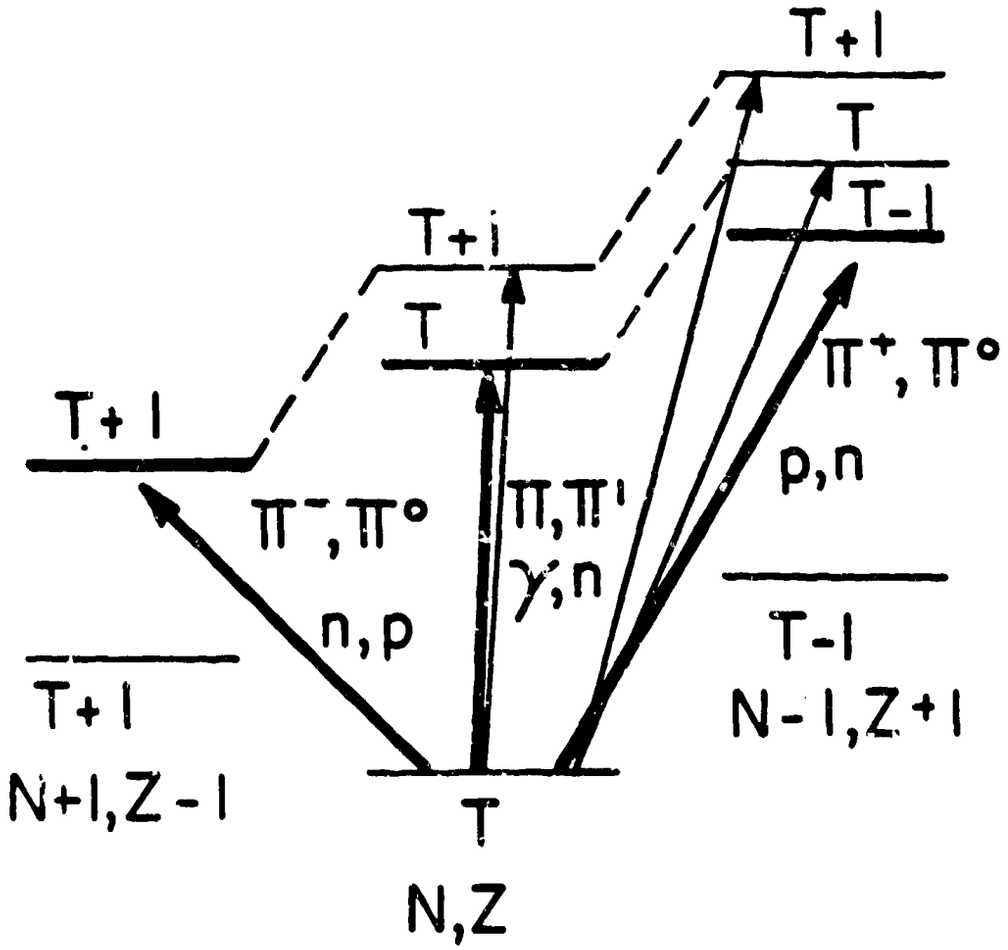

Fig 2

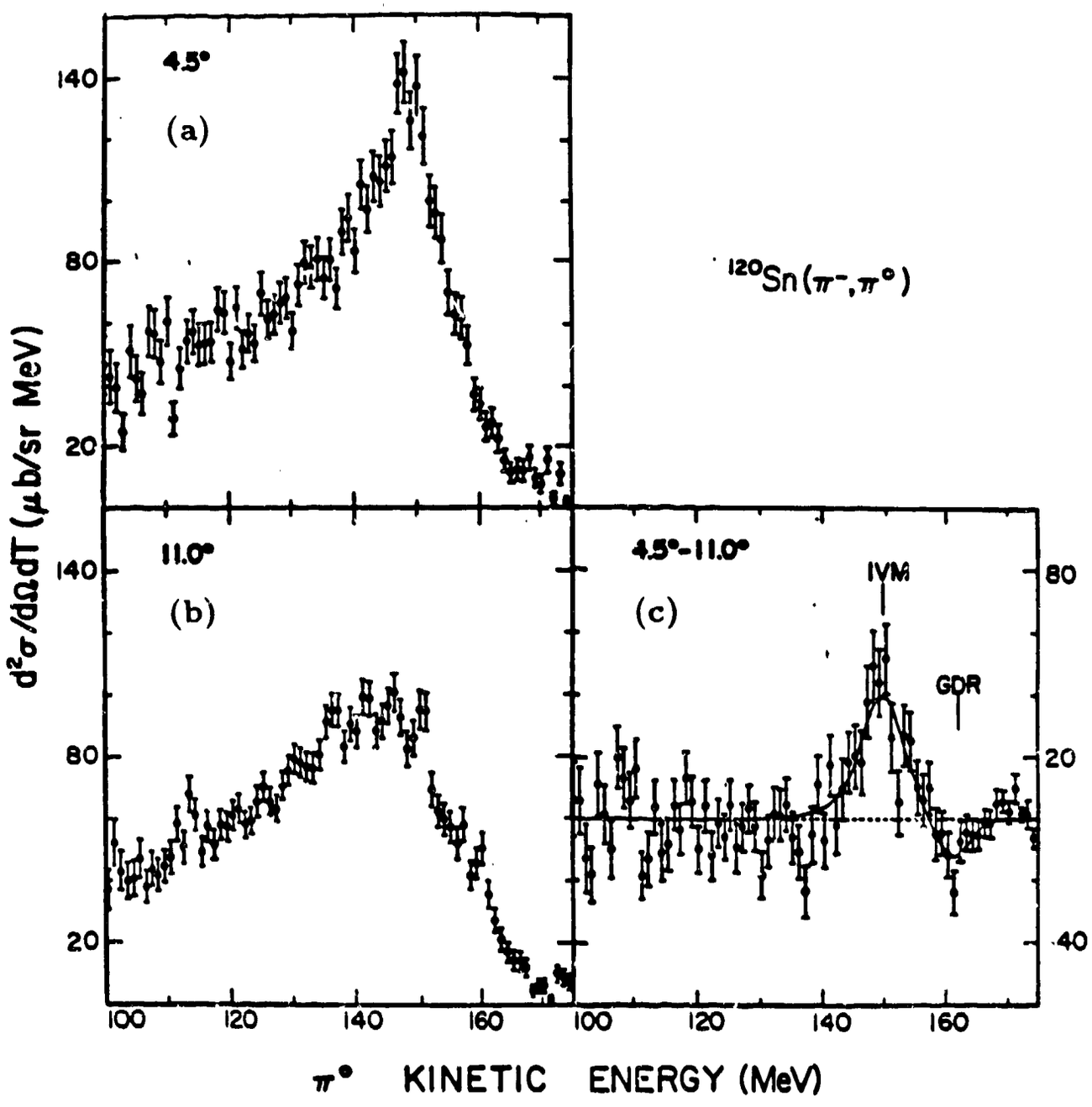
4.5°
(a)
11.0°
(b)
4.5°-11.0°
(c)
IVM
GDR
$^{120}Sn(\pi^-,\pi^0)$
$d^2\sigma/d\Omega dT$ (μb/sr MeV)
π^0 KINETIC ENERGY (MeV)
140
80
20
100
120
160
40

Fig 3

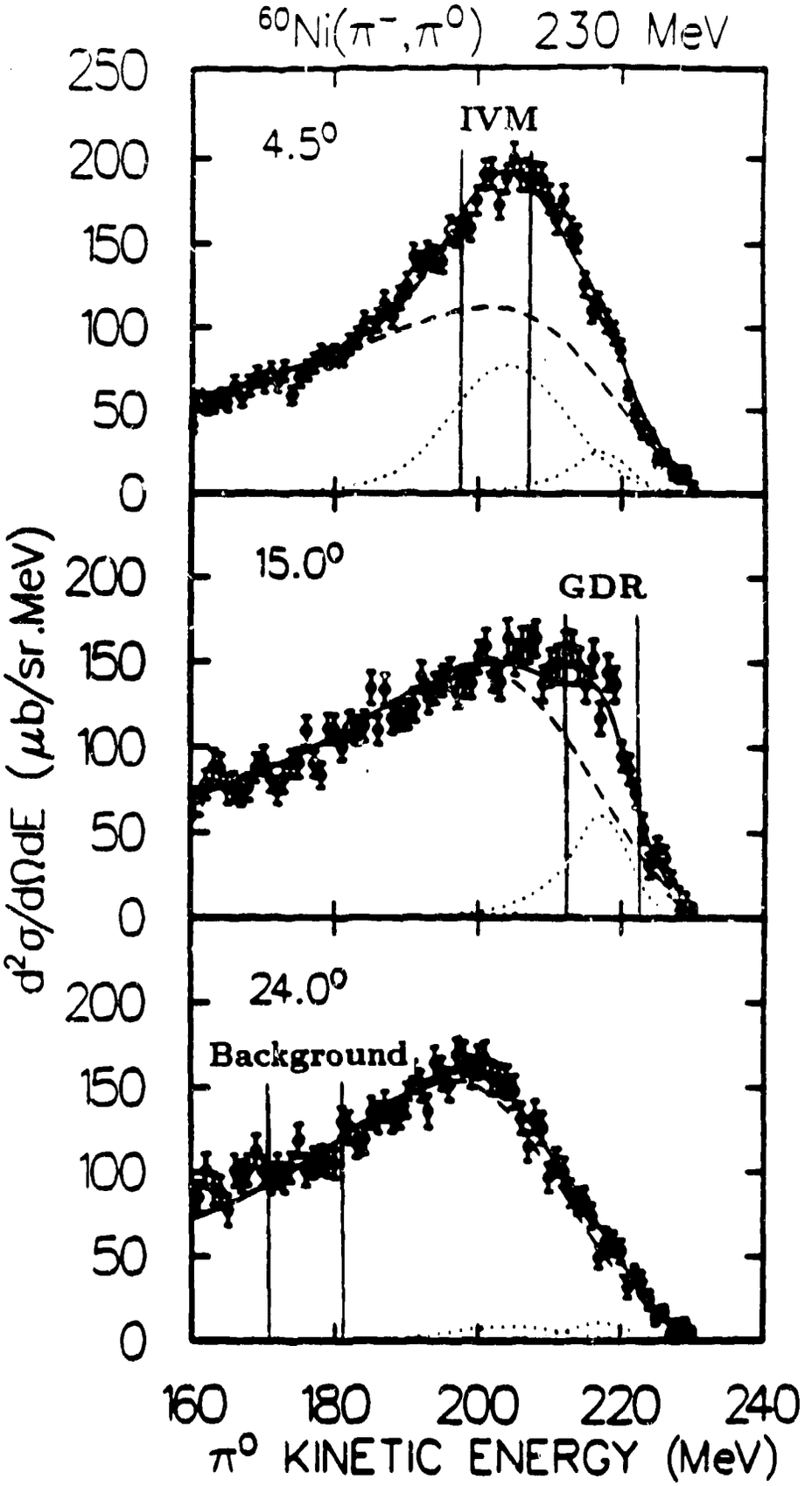
$^{60}Ni(\pi^-,\pi^0)$ 230 MeV
4.5°
IVM
15.0°
GDR
24.0°
Background
$d^2\sigma/d\Omega dE$ (μb/sr.MeV)
250
200
150
100
50
0
160
180
200
220
240
π^0 KINETIC ENERGY (MeV)

Fig 4

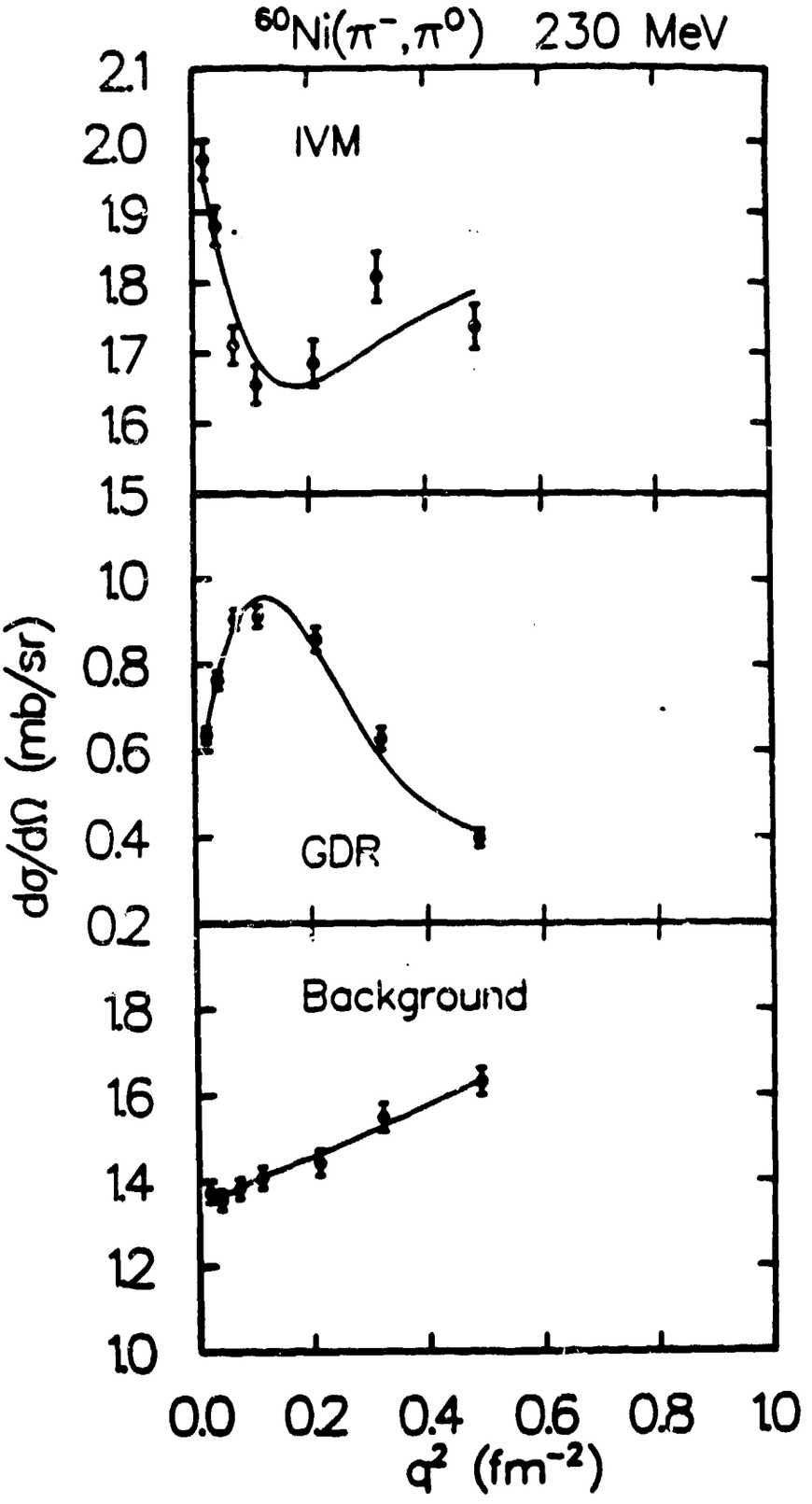
$^{60}Ni(\pi^-,\pi^0)$ 230 MeV
IVM
GDR
Background
$d\sigma/d\Omega$ (mb/sr)
q^2 (fm^{-2})
2.1
2.0
1.9
1.8
1.7
1.6
1.5
1.0
0.8
0.6
0.4
0.2
1.8
1.6
1.4
1.2
1.0
0.0
0.2
0.4
0.6
0.8
1.0

Fig 5

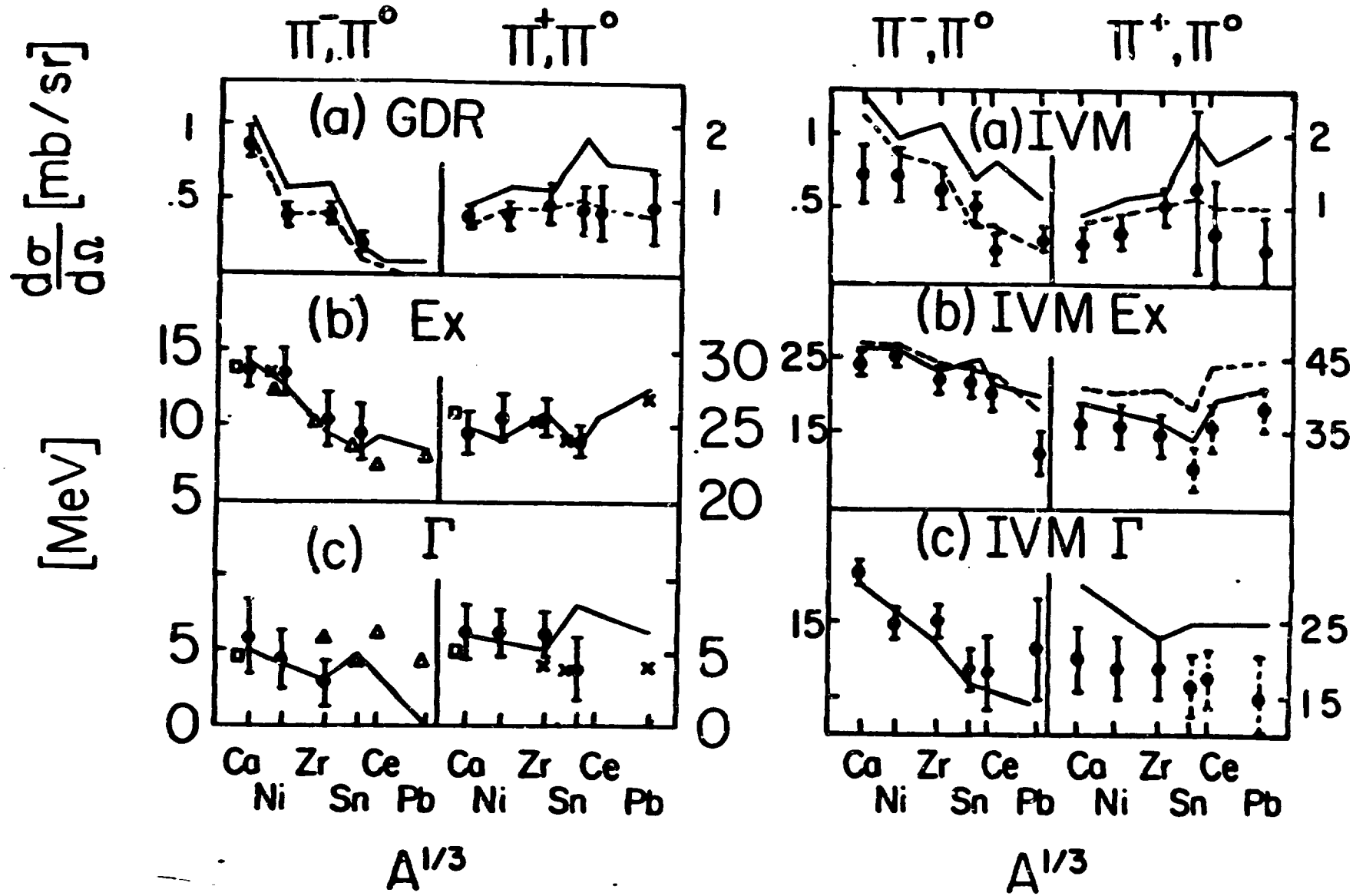
π⁻,π°
π⁺,π°
(a) GDR
(b) Ex
(c) Γ
dσ/dΩ [mb/sr]
[MeV]
1
.5
2
1
15
10
5
0
30
25
20
5
0
Ca Zr Ce Ca Zr Ce
Ni Sn Pb Ni Sn Pb
A^1/3
π⁻,π°
π⁺,π°
(a)IVM
(b) IVM Ex
(c) IVM Γ
1
.5
2
1
25
15
45
35
15
25
15
Ca Zr Ce Ca Zr Ce
Ni Sn Pb Ni Sn Pb
A^1/3

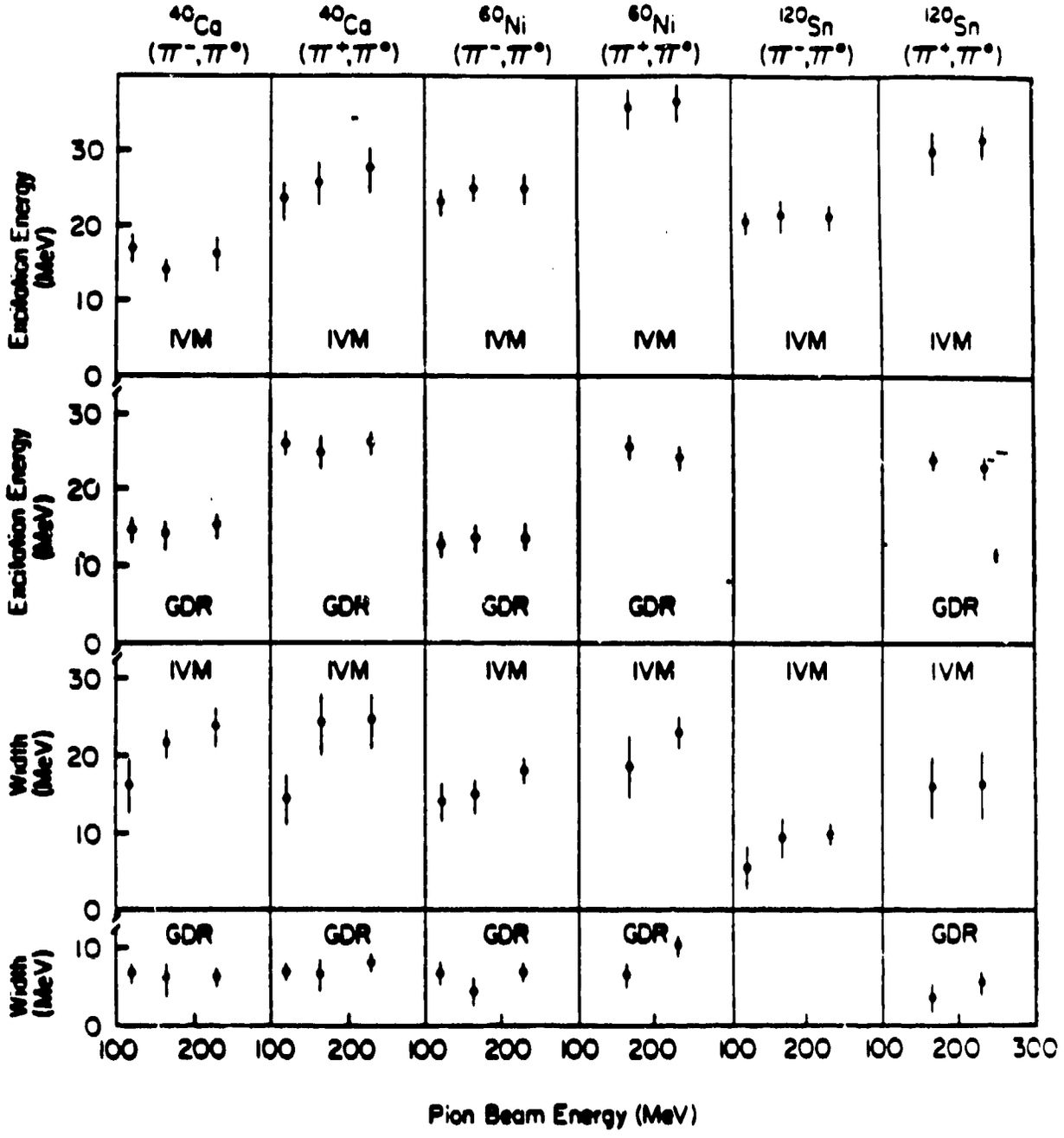
^{40}Ca (π^-,π^0)
^{40}Ca (π^+,π^0)
^{60}Ni (π^-,π^0)
^{60}Ni (π^+,π^0)
^{120}Sn (π^-,π^0)
^{120}Sn (π^+,π^0)
Excitation Energy (MeV)
Width (MeV)
IVM
GDR
0
10
20
30
100
200
300
Pion Beam Energy (MeV)

Fig 7

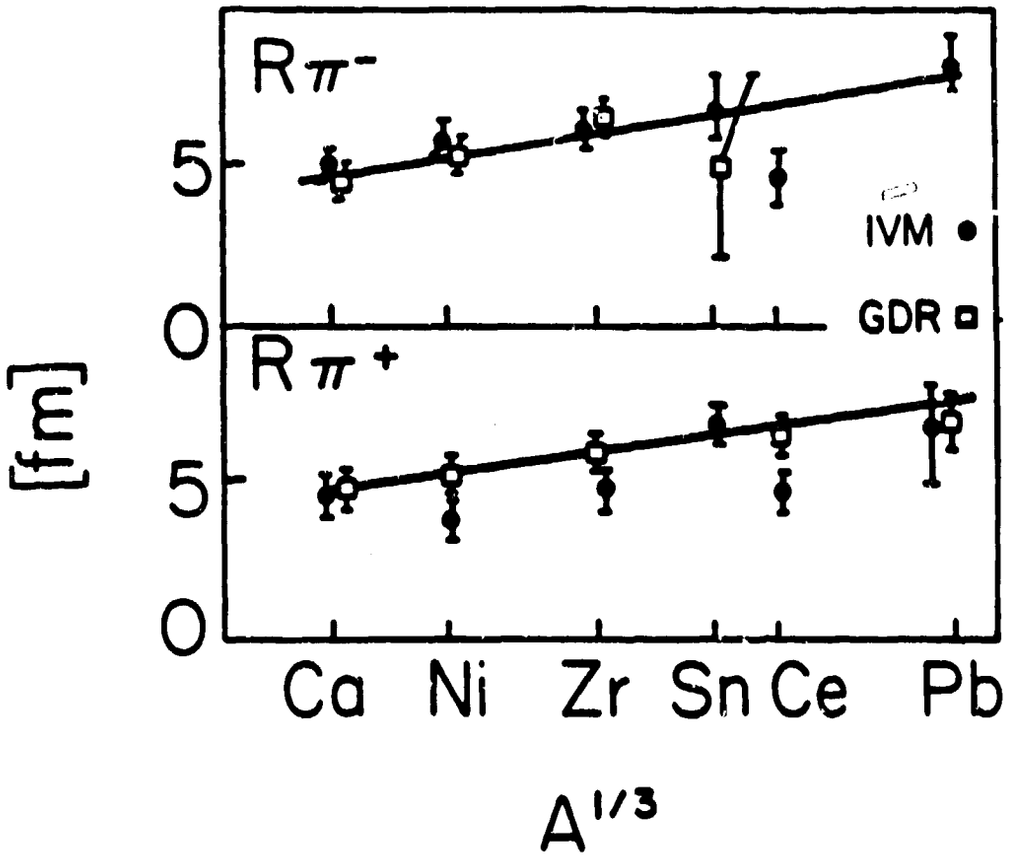

Fig 8

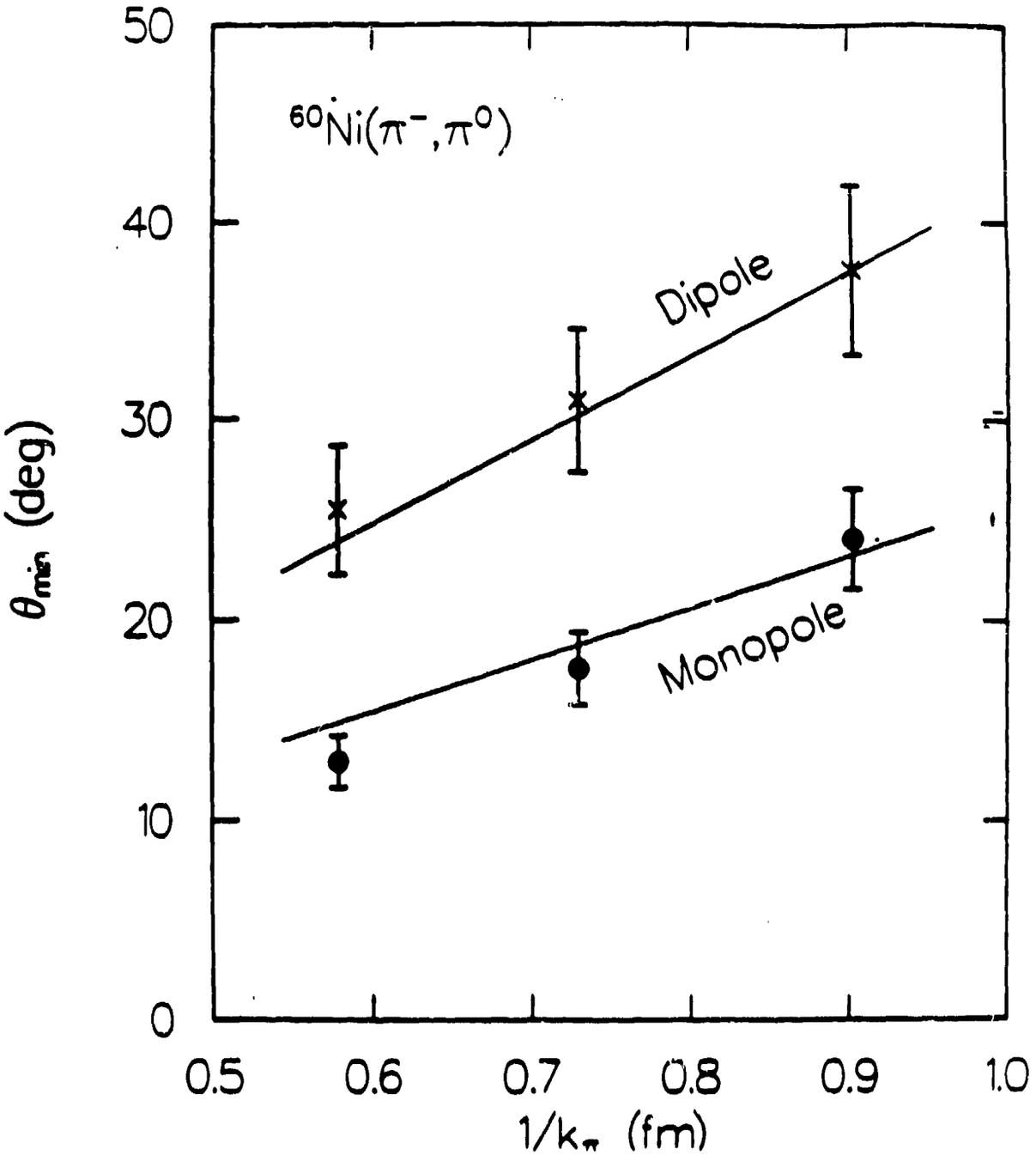
50
40
30
20
10
0
$^{60}Ni(\pi^-,\pi^0)$
Dipole
Monopole
θ_{min} (deg)
0.5
0.6
0.7
0.8
0.9
1.0
$1/k_\pi$ (fm)

Fig. 9

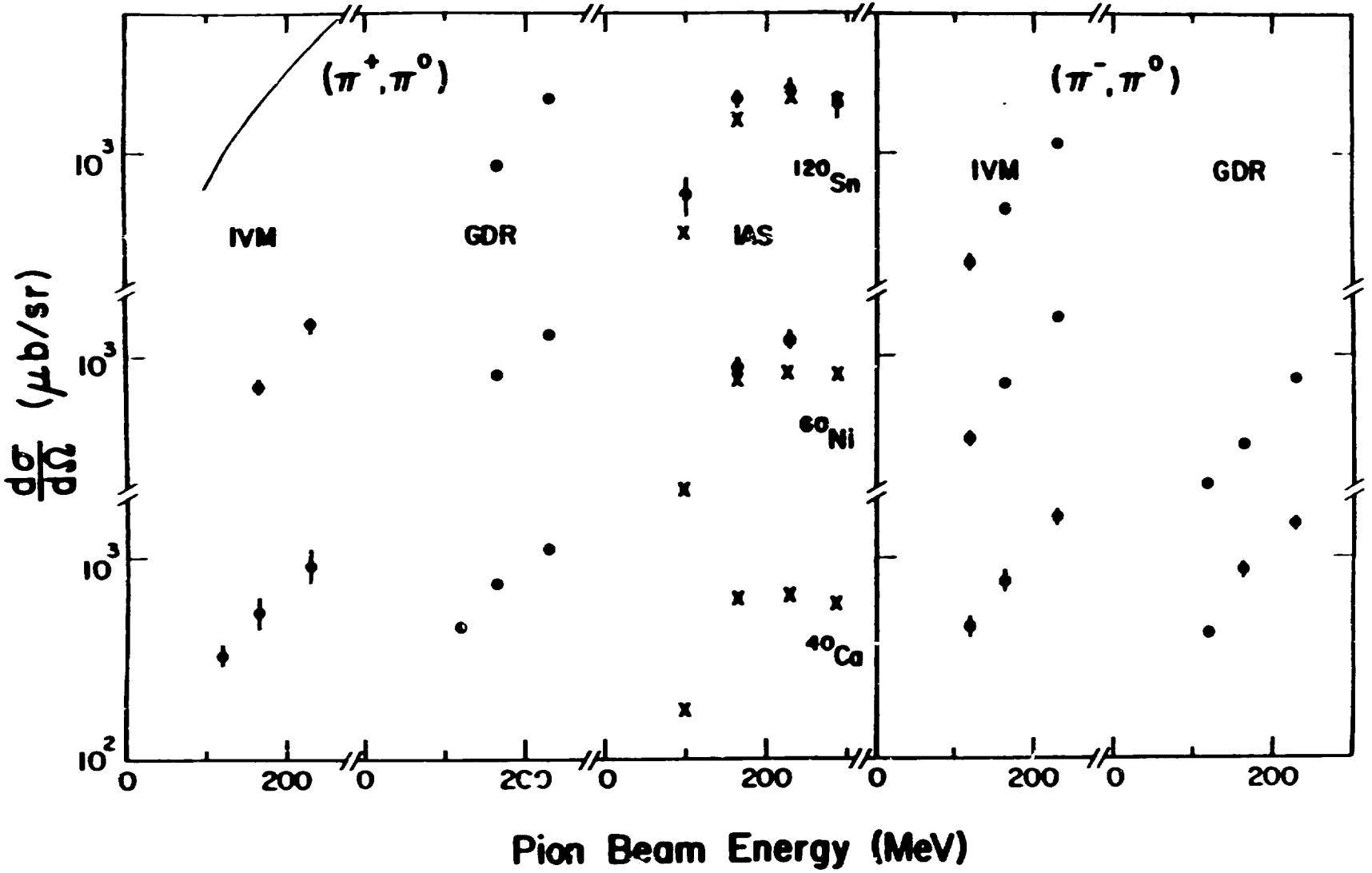
(π^+,π^0)
(π^-,π^0)
IVM
GDR
IAS
IVM
GDR
^{120}Sn
^{60}Ni
^{40}Ca
10^3
10^3
10^3
10^2
0
200
0
200
0
200
0
200
$\frac{d\sigma}{d\Omega}$ (μb/sr)
Pion Beam Energy (MeV)

Fig. 5 10